Practical Atmospheric Correction Algorithms for a Multi-Spectral Sensor from the Visible through the Thermal Spectral Regions

Christoph C. Borel, Pierre V. Villeneuve, William B. Clodius,
John J. Szymanski and Anthony B. Davis
Space and Remote Sensing Sciences Group
NIS-Division, Mailstop C323, Los Alamos National Laboratory
Los Alamos, NM 87545, USA
cborel@lanl.gov

ABSTRACT

Deriving information about the Earth's surface requires atmospheric corrections of the measured top-of-the-atmosphere radiances. One possible path is to use atmospheric radiative transfer codes to predict how the radiance leaving the ground is affected by the scattering and attenuation. In practice the atmosphere is usually not well known and thus it is necessary to use more practical methods. We will describe how to find dark surfaces, estimate the atmospheric optical depth, estimate path radiance and identify thick clouds using thresholds on reflectance and NDVI and columnar water vapor. We describe a simple method to correct a visible channel contaminated by a thin cirrus clouds.

Keywords: Atmospheric correction, multi-spectral algorithms, water vapor retrieval, cloud detection, cirrus correction

1. Introduction

There are many methods to generate atmospherically corrected surface reflectances in the solar part of the spectrum for multi-spectral and hyper-spectral sensors. We list a few multi-spectral atmospheric correction (AC) methods known to the authors:

- Dark target (Chavez, 1988, Teillet et al, 1995),
- Spectral channel correlation approaches (Liang, 1997),
- Match retrieved ground reflectances to spectral libraries (ATCOR2 (Richter, 1996)),
- Correct for adjacency effect and terrain effects (Richter, 1998),
- Atmospheric pre-corrected differential absorption to retrieve columnar water vapor over dark targets (APDA, e.g. Schlaepfer and Borel, 1998),
- ATmosphere REMoval Program (ATREM) (Gao, 1993a),
- Second Simulation of the Satellite Signal in the Solar Spectrum (6S) (Vermote, 1996),
- Moderate Resolution Model for LOWTRAN7 (MODTRAN) (Kneizys, 1995)
- Multiple temporal looks and fractal dimension analysis (Tornow, 1993), and
- Multiple angular views (Diner et al, 1989).

A systematic comparison of many of the above methods can be found in O'Neill et al, 1995. The list is much shorter for multi-spectral thermal atmospheric corrections to retrieve land surface temperatures and emissivities:

- Multi-look techniques for water surfaces (Tornow et al, 1994),

- Known emissivity for a channel (Kahle et al, 1980),
- Alpha residuals method (Hook et al, 1992),
- Minimum maximum difference (MMD) (Gillespie et al (1996)),
- Spectral smooth emissivity method for hyper-spectral sensors (Borel, 1996), and
- Physics-based sea surface temperature retrieval (Borel et al, 1999).

In a paper in this conference we cover more details on atmospheric corrections in the thermal, see Borel et al, 1999. Many of the algorithms have either not been validated or have been validated on very limited data sets. The algorithms all have strengths and weaknesses. The methods are usually very sensor and scene specific. We know of no existing codes which are easy to use. Codes like ATREM, MODTRAN and 6S require substantial user training and are difficult to apply if the atmospheric conditions are not known. Some of the algorithms include advanced features like the inclusion of bi-directional reflectance distribution functions and adjacency effects. The advanced algorithms require many additional pieces of information usually not available to the user. Furthermore, AC algorithms will depend on what products the user is interested to generate. For example, if the user is interested in improved atmospherically corrected vegetation indices, it might be unnecessary to use an advanced AC algorithm. Some vegetation indices, such as the GEMI (Pinty and Verstraete, 1992) are specifically formulated to mitigate atmospheric effects. However, if the application is the retrieval of phytoplankton concentration or bathymetry, advanced radiative transfer codes should be used to estimate the atmospheric path radiance and extinction. In practice we found that the AC algorithm is tightly coupled to applications and that the notion of treating AC's as a separate research topic is misleading.

We have also not found much written about how to use the scene image itself to estimate atmospheric parameters. The usual assumption is that these parameters can either be guessed somehow (e.g. ATREM, 6S) or be obtained from other data such as radiosonde profiles (MODTRAN). In this paper we discuss a few potential in-scene pre-processing algorithms which could be used before an AC is performed. We show two practical AC methods and results using multi-spectral scenes simulated from AVIRIS data, where the atmospheric conditions are not known.

2. Pre-processing algorithms for in-scene atmospheric corrections

Atmospheric corrections can often make use of the following intermediate products:

- Dark target recognition: to identify atmospheric radiances minimally contaminated by surface radiance.
- Water and dark vegetation masks: to identify regions where the spectrum may be easy to model.

Finally we need to screen for clouds.

2.1. Finding dark targets

One of the simplest tasks is to locate dark targets in a scene. The simplest algorithm for this task is to set a threshold for the apparent reflectance ρ^* which will depend on the atmospheric turbidity. The apparent reflectance is given by:

$$\rho^* = \frac{L_m}{\pi\mu \int_{\lambda_1}^{\lambda_2} R(\lambda)E_0(\lambda)d\lambda}, \tag{1}$$

where L_m is the measured radiance, μ is the cosine of the angle between the sun and the surface normal, $R(\lambda)$ is the sensors response between wavelengths λ_1 and λ_2 and $E_0(\lambda)$ is the solar irradiance. So a simple method to find a dark surface indicator $I_{i;dark}$ for channel i is:

$$I_{i;dark}(t) = \rho_i^* < t\ min(\rho_i^*), \tag{2}$$

where t is somewhat greater than 1. If a dark surface for more than one channel is to be found we can use logical combinations such as:

$$I_{1,3,5;dark} = I_{1;dark}(t_1) \cap I_{3;dark}(t_3) \cap I_{5;dark}(t_5). \tag{3}$$

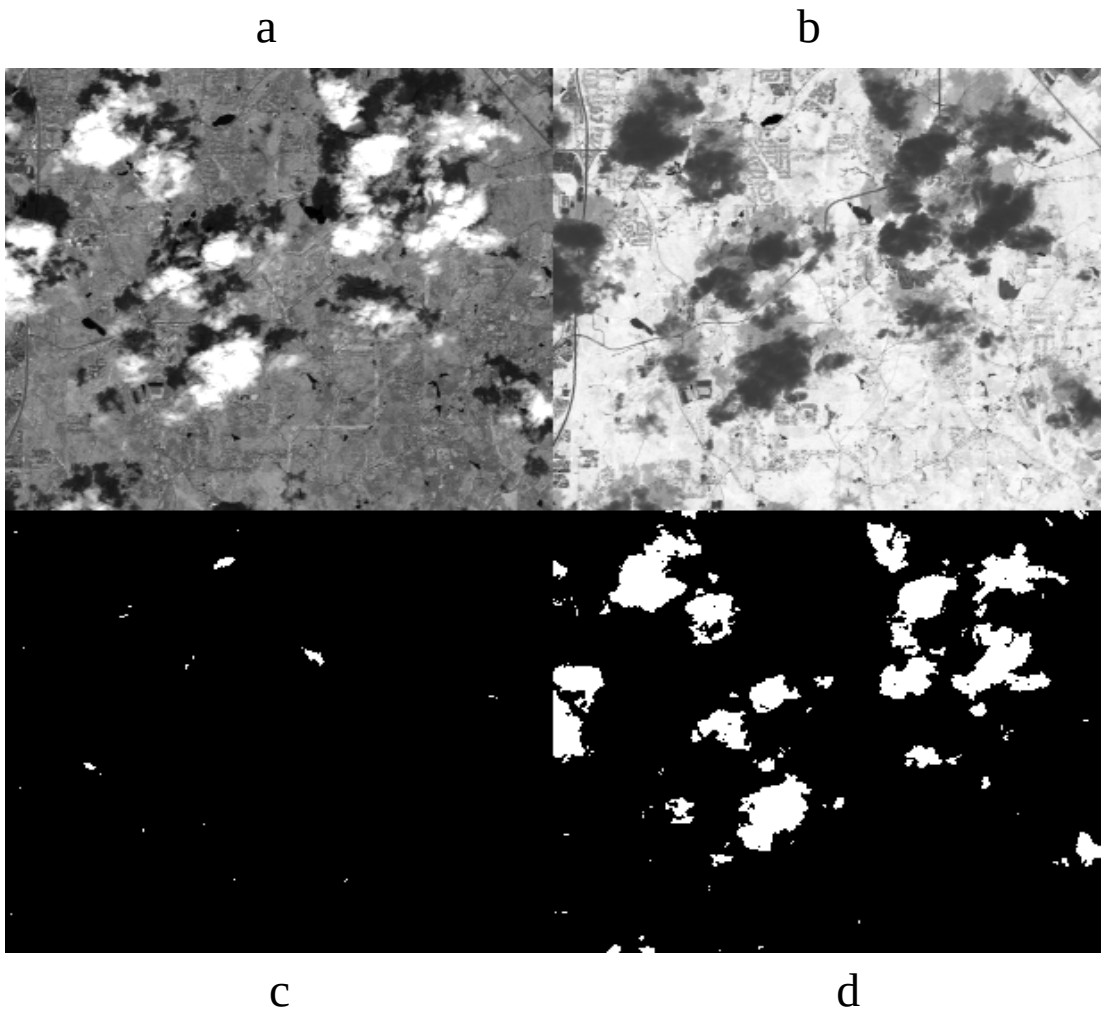

Figure 1. (a) AVIRIS derived reflectance image in NIR channel, (b) NDVI, (c) water mask and (d) cloud mask.

2.2. Water masks

Water can be found using the dark target approach or a slightly more sophisticated version based on the normalized difference vegetation index (NDVI) combined with a reflectance threshold:

$$I_{red,nir;water}(t_{ndvi}, t_{red}) = \frac{\rho^*_{nir} - \rho^*_{red}}{\rho^*_{nir} + \rho^*_{red}} < t_{ndvi} \cap \rho_{red} < t_{red}. \quad (4)$$

In Figure 1 we show a scene derived from AVIRIS data (970806t01p02_r07_sc04) where we applied the water mask using a threshold of t_{ndvi}=0.041 and $t_{red} = 0.3$ using TOA reflectance data.

2.3. Screening of clouds

In land-surface remote sensing with high-precision VIS/NIR radiometry, in the absence of clouds radiances are converted to ground reflectance assuming directly transmitted illumination by solar rays and diffuse illumination by down-welling sky radiance. If there is any significant cloud in the vicinity of the target, the inferred surface reflectance will be in error. It is therefore necessary to identify clouds in the scene and cloudy pixels need to be systematically "flagged" so that end-users of the remote sensing data are alerted to potential corruption of retrieved surface reflectance.

There are several well-documented techniques for discriminating optically thick cloud masses using multi-spectral imagery and new ideas are being investigated. Their physical basis is that optically thick clouds are almost invariably brighter in the visible and NIR. In the thermal infrared clouds are usually colder than the surface, which is true for low-level liquid clouds having an emissivity close to unity and high-level ice clouds. So the most widely used cloud masking techniques involve thresholds in spectral albedo and/or brightness temperature (the latter only at night). In the reflection-based method, the NDVI has been shown to be a robust cloud discriminator because of their inherent whiteness. The following equation can be used to generate cloud masks:

$$I_{red,nir;cloud}(t_{ndvi}, t_{nir}) = \frac{\rho^*_{nir} - \rho^*_{red}}{\rho^*_{nir} + \rho^*_{red}} < t_{ndvi} \cap \rho_{nir} > t_{nir}, \tag{5}$$

where we find that typical values for the thresholds are $t_{ndvi} \approx 0.1$ and $t_{nir} = 0.3$. In Figure 1 (d) we show a cloud mask using a threshold of t=0.13 applied to TOA reflectance data. Once pixels have individually been classified as cloudy or not, it is recommended to re-scan the images and "fill-in" cloudy areas based on a neighboring-pixel criterion since radiance from surface viewed through a gap in cloudiness is unlikely to be quantitatively usable.

Detection of cloud shadows is equally important from the standpoint of a quantitative analysis of surface radiance, because the normally dominant source of illumination (direct beam transmission) is all but extinguished. Unsupervised identification of cloud shadow is more difficult than finding cloud in the line-of-sight. Fortunately, most dense cloud masses are at a low enough altitude (a few km) that one will see both a cloud and its shadow in typical images (even at quite high spatial resolutions).

Clouds can be detected using a water vapor "slicing" technique. Because most water vapor is below the cloud layer, clouds actually appear "dry". We have applied the method proposed by Gao and Goetz, 1991, to produce cloud masks. The following equation is often called continuum interpolated band ratio (CIBR) (e.g. Schlaepfer et al, 1998) is a simple ratio of the measured TOA radiances L_i reference channels (1 and 3) to a measurement channel (2):

$$CIBR(L_1, L_2, L_3) \; = \; \frac{L_1 + L_3}{2\, L_2}. \tag{6}$$

See Fig. 3 for an illustration using some low lying clouds over mostly bright vegetation covered surface. The atmosphere above the cloud has a small columnar water vapor amount, thus the CIBR is smaller than over clear sky areas.

While this paper is on atmospheric corrections we digress a little to present an exciting finding of what we believe are due to multiple scattering effects near cloud boundaries. Notice in Figure 3-b that the cloud shadows appear to have more columnar water vapor than the illuminated surface. We believe that some of the sun-shaded surface is illuminated by diffusely transmitted light from the cloud. See Figure 2 for a diagram of the discussed photon paths. Photons in the water absorption band are more attenuated by the water vapor in the cloud than the reference channels. A probably negligible part of the increased columnar water vapor may be due to multiple scattered photons from outside the cloud who travel longer paths through the atmosphere, thus encountering more water vapor. There also seems to be an extended area of increased columnar water vapor of the sunlit side of the central cloud which could be explained by photons multiply scattered inside the cloud to the surface and back to the sensor, encountering more water vapor absorption along the way than just a pass from the sun to surface to sensor.

Tenuous high-level clouds (sub-visual cirrus) offer a different challenge; optically akin to an aerosol layer far above the surface, their effect on path radiance can potentially be removed if they are properly identified. For optically thin high-level clouds, Gao et al., 1993b have proposed to use a dedicated channel at 1.38 μm in a deep water vapor absorption band. At this wavelength, the moist lower troposphere acts essentially as a strong absorber, so that the observed radiance is attributable to scattering particles in the upper troposphere and stratosphere, where cirrus occur. Of course, this technique will not work as well in high and/or dry regions of the globe.

Using AVIRIS data provided by Gao over Coffeyville, KS , based on Gao's ideas (Gao et al, 1998) a very simple visual correction algorithm for cirrus clouds can be applied:

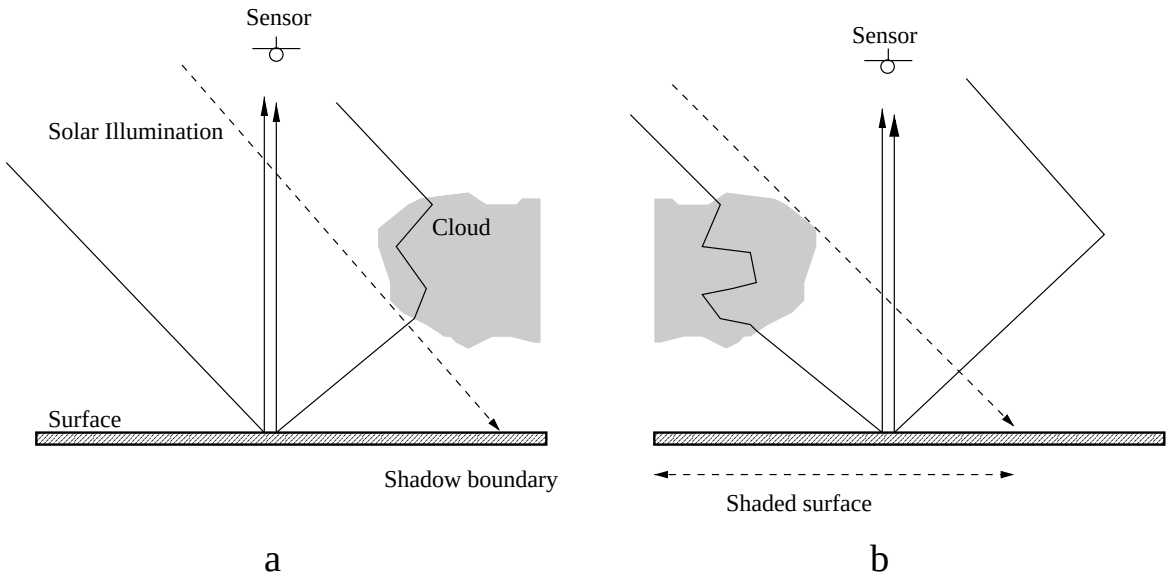

Figure 2. (Photon paths explaining an apparent enhanced columnar water amount seen in Figure 3 for a) above surface surrounding a cloud and b) in the cloud shadow.

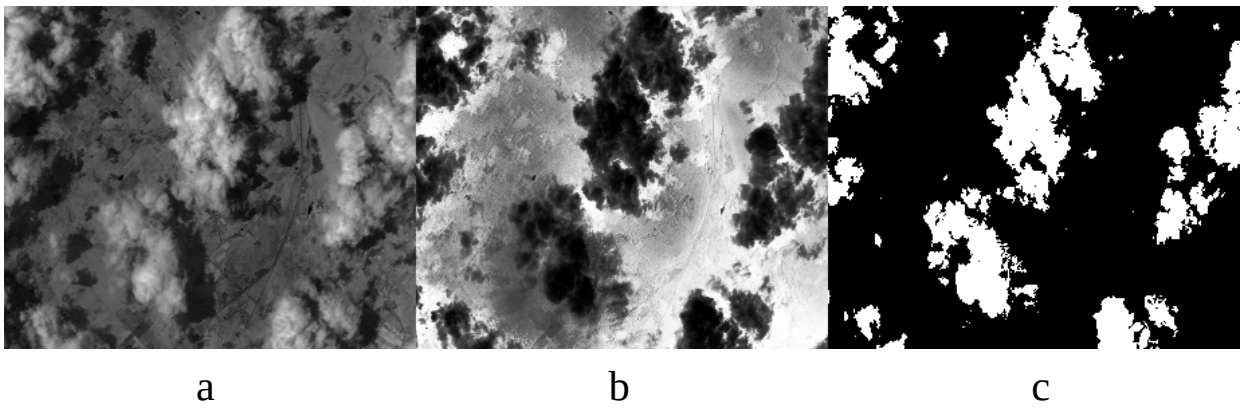

Figure 3. AVIRIS derived reflectance image in (a) NIR channel and (b) histogram equalized continuum interpolated band ratio (CIBR) which if thresholded yields (c) the cloud mask.

a b c

Figure 4. Histogram equalized images of (a) 1.38 μm channel with a visible cirrus cloud, (b) channel 17 (0.547 μm) visible channel with cirrus cloud contamination and (c) cirrus corrected channel 17.

1. Perform a linear regression of channel 17 digital numbers (DN's) versus channel 111 (the 1.38 μm channel: $DN_{17} = 547 + 6.2\ DN_{111}$.
2. Approximate the corrected visible channel using:

$$DN_{17;corrected}(x,y) = DN_{17}(x,y) - 600. - 6.2\ smooth(DN_{111}(x,y), 21),$$

where *smooth*() is a 21 x 21 rectangular smoothing filter which smoothes the inherently noisy 1.38 μm data. We choose 600 as an offset to include most of the correlated samples.

In Figure 4 we show an example of the kind of results which can be obtained with a simple cirrus correction algorithm. Note that this simple algorithm does not account for transmission losses through the atmosphere or attenuated sunlight from other parts of the cirrus cloud.

3. Aerosol Correction for Reflectance Using In-Scene Information

The two algorithms described below rely on in-scene information to characterize the aerosol content of the atmosphere, and use this same information to correct for the presence of the aerosol and the remaining atmosphere.

3.1. Atmospheric correction over dark vegetation

There are two important steps to any operational atmospheric aerosol correction algorithm: 1) the retrieval of the atmospheric optical properties from special regions of the imagery itself; and 2) calculating the surface reflectance from the TOA reflectances and retrieved parameters. In this algorithm, the only variable that is estimated from the image directly is the aerosol optical depth. Other parameters are defined by the assumed aerosol type and climatological conditions (Mid-latitude summer, etc.). Other parameters needed to run an atmospheric model are readily known or can be easily computed, such as the solar illumination and sensor viewing geometries and atmospheric Rayleigh optical depth. However, the aerosol optical depth varies significantly, both spatially and temporally and must be determined on a scene-specific basis. An atmospheric correction over dense dark vegetation is shown in a flow diagram in Figure 5. The first step estimates the surface reflectance in dark pixels over vegetation pixels at 0.50 and 0.66 μm. This step is needed to place lower bounds on the atmospheric radiance. A good estimate for the surface reflectance is to identify dark materials, which have well known reflectances, and use values from a spectral library. It is important to locate dark regions because in these regions the majority of the measured signal will consist of molecular and aerosol-scattered radiance (path radiance). Dark targets with very low reflectance in the visible region are useful in this application, because any uncertainties in the assumed dark target reflectances will have a minimal effect on the retrieved aerosol optical thickness (Teillet and Fedosejevs, 1995). Thus the TOA measurement is most closely related to the desired aerosol optical depth. Kaufman et al., 1996, have found a strong correlation between the surface reflectances at 2.1 μm and 0.50 μm

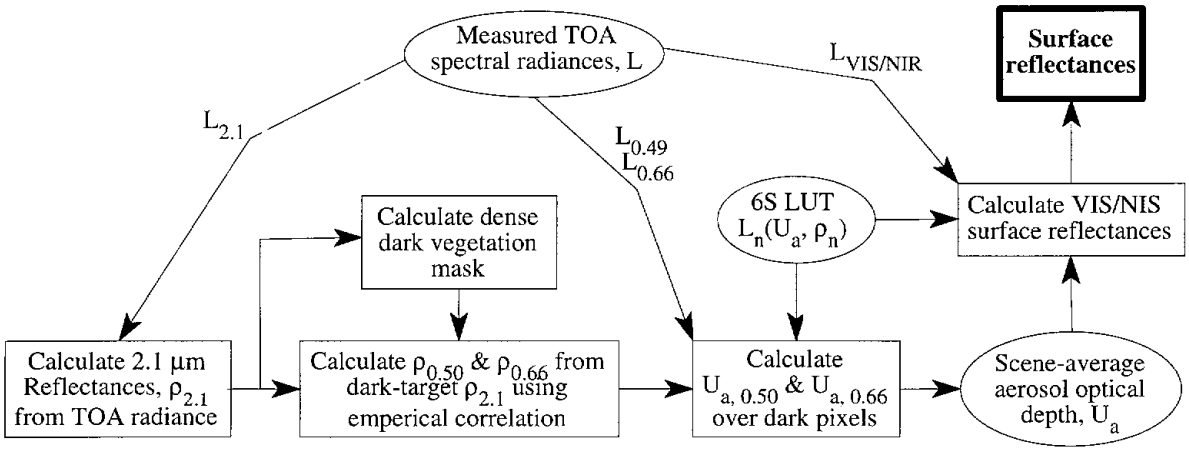

Figure 5. Flow diagram of the atmospheric correction algorithm based on dense dark vegetation.

as well as between 2.1 μm and 0.66 μm. The atmosphere is effectively transparent (including water vapor and aerosols) at 2.1 μm, thus this correlation can be used to predict surface reflectance at 0.50 and 0.66 μm from reflectance measurements at 2.1 μm for dense dark vegetation and dark soil regions in the scene of interest.

Dark regions in general can be found by thresholding the 2.1 μm reflectances below 0.15. Dense vegetation can be found by finding NDVI values greater than a threshold of approximately 0.5. The NDVI in this case must be calculated from TOA reflectances since the surface reflectances have not yet been determined. However, this is not a problem since the effect of aerosols is to reduce NDVI by reducing the relative contrast between red and NIR wavelengths. This can be approximately compensated by using a slightly larger value for the NDVI threshold. Once these regions of dense vegetation and dark soil have been located, the above-mentioned correlation can be used to estimate their 0.50 and 0.66 μm reflectances.

At this point an assumption is made that the only unknown for the dark soil and dense vegetation pixels is the atmospheric aerosol optical depth. The other major atmospheric properties can be obtained elsewhere, e.g. Rayleigh scattering from standard atmospheric profiles and water vapor column density from an independent algorithm operating in a different spectral region (NIR). Given the surface estimated reflectance and the top of the atmosphere measured reflectance, the aerosol optical depth can be retrieved with a comprehensive look up table (LUT) relating TOA reflectance to surface reflectance, aerosol depth, water content, viewing angle, solar angle, etc. This LUT can be generated from any number of available atmospheric models (MODTRAN, 6S, etc.). An example of the TOA reflectances computed for a LUT is shown in Figure 6. This Figure shows TOA reflectance as a function of surface reflectance and aerosol optical depth (20 deg. solar angle, nadir observation, mid-latitude summer atmosphere with marine aerosol type). Notice the slight curvature for higher values of surface reflectance, this is due to the multiple scattering between the surface and atmosphere. Also there is a surface reflectance $\rho_{critical}$ near 0.2 where all curves nearly meet which occurs when scattering contributions cancel the transmission losses. More details on the critical reflectance can be found in Fraser and Kaufman, 1985. An example of using this LUT to predict aerosol optical depth is done with an AVIRIS scene of Camarillo, CA, resampled to the 10 visible and NIR MTI channels (A - I, and O). The scene in band A (0.45-0.52 μm) is shown in Figure 7-a. A mask for dense dark vegetation and dark soils is found by thresholding the 2.2 μm TOA reflectance (MTI band O (2.08-2.37 μm)) for pixels below 0.15. This result is shown in Figure 7-b. For each of these masked pixels the aerosol optical depth is estimated using the LUT procedure discussed above. The average optical depth value over this scene was found to be $\tau = 0.20$.

The next step is to use this aerosol optical depth value to predict the surface reflectance over the entire scene

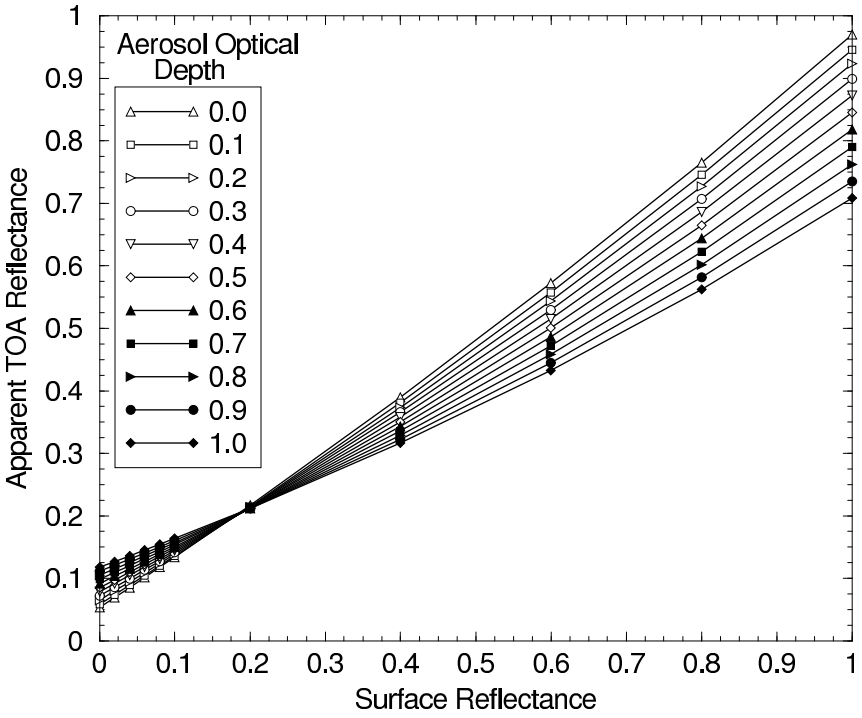

Figure 6. Top of atmosphere radiances for the blue channel (0.45-0.52 μm) as a function of aerosol optical depth.

using the same LUT. In this case, the unknown is the surface reflectance instead of the aerosol optical depth. The aerosol-corrected version of the Camarillo scene is shown in Figure 7-c. Notice that in comparison with the uncorrected image there is much stronger contrast between the light and dark regions in the scene. The difference between the corrected and uncorrected is shown in Figure 7-d. This difference is largest over mountain slopes and certain agricultural fields because it is over these dark areas that the atmospheric path radiance is most significant.

3.2. Atmospheric correction over water

Another practical atmospheric correction algorithm uses apparent reflectances in several channels over water to fit a simple empirical relationship. The algorithm has the following steps:

1. Select dark water pixels from a multi-spectral image, e.g. Landsat channels. We use an interactive method changing the threshold t in eq.(4) until the desired water bodies are found. The water mask is used to find the darkest pixel in each channel. Alternatively the user can also select a particular pixel manually.

2. Perform a linear fit to the minimum apparent reflectances $\rho^*_{i;min}$, $i = 1,2,3$ with $y = a_{vis} + b_{vis}x$ for $x_i = \log_{10}(\lambda)$ and $y_i = \log_{10}\rho^*_i$, where $i = 1,2,3$ are the visible blue, green and red channels.

3. Perform a linear fit to the minimum apparent reflectances $\rho^*_{i;min}$, $i = 4,5,7$ with $1y = a_{swir} + b_{swir}x$ for $x_i = \log_{10}(\lambda)$ and $y_i = \log_{10}\rho^*_i$, where $i = 4,5,7$ are the short-wave infrared .8, 1.65 and 2,2 μm channels.

4. Compute the atmospheric path reflectance corrected ground reflectance using the fitting coefficients from steps 2 and 3: $\rho^*_{i;corrected} = \rho^*_i - \rho_{i;path}$, where $\rho_{i;path} = 10.^{a+b\ \log_{10}(\lambda_i)}$.

5. Check for negative apparent corrected reflectances $\rho^*_{i;corrected}$ and repeat steps 2 and 3 if necessary choosing a different set of pixels by varying the threshold to determine the water surfaces.

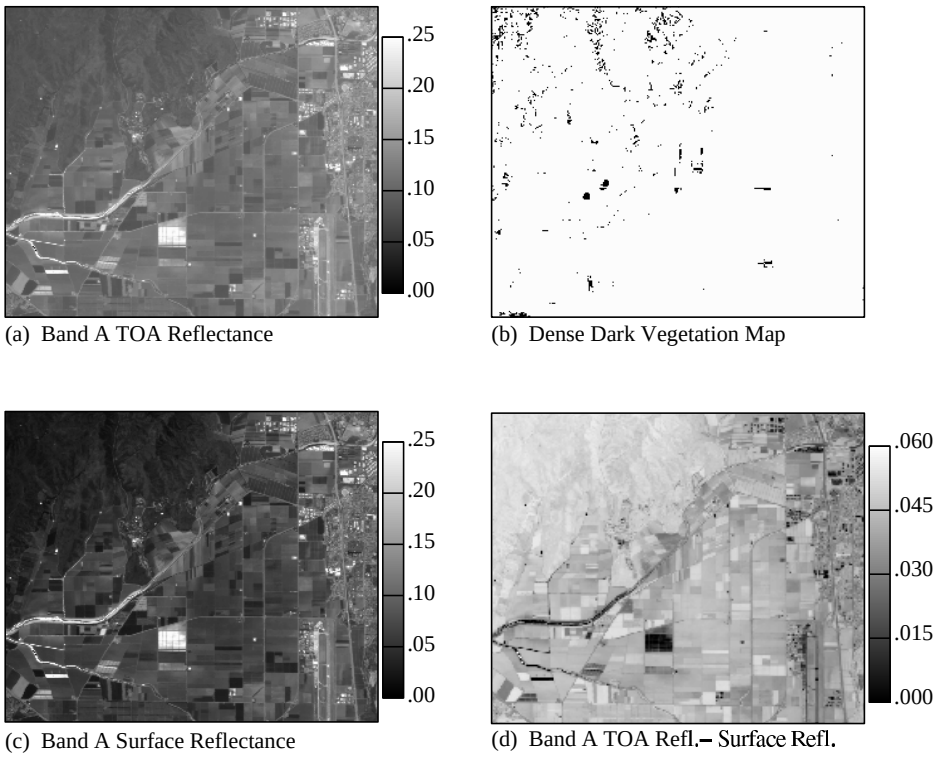

(a) Band A TOA Reflectance

(b) Dense Dark Vegetation Map

(c) Band A Surface Reflectance

(d) Band A TOA Refl.– Surface Refl.

Figure 7. Example (a) TOA, (b) dense dark vegetation, (c) ground reflectance and (d) reflectance error images for blue channel over Camarillo, CA.

Note that we neglect the transmission of the atmosphere using this simple approach. We are currently working on an approach which uses the fitting coefficients from steps 2 and 3 to actually find the total transmission based on either 6S or MODTRAN calculations.

The correction for the transmission is just a scaling factor. From a practical standpoint it seems that with all the additional uncertainties of present remote sensing sensors (noise, calibration, quantization limits,...), complicating factors (e.g. local terrain slopes, adjacency effect, BRDF effects,...) and modeling limits, this is an acceptable route.

Over large bodies of near-shore water we found a typical exponent b_{vis} and b_{swir} in the order of -4, which is indicative of Rayleigh scattering. In other papers the exponent b is sometimes called the "Armstrong" exponent. Figure 8 shows how the path reflectance in a log-log plot falls of with increasing wavelength. The horizontal bars indicate the location of MTI bands A-I and O. All except F and H are located in atmospheric windows and show a remarkable linear relationship with respect to wavelength in the log-log plot. Over smaller reservoirs and ponds we found b_{vis} tended to be larger than b_{swir} and ranges from -1.5 to 3.5. We believe that this is due to suspended sediments and/or algae in the water. Calculations using MODTRAN showed that these corresponded to atmospheres with variable amount of aerosol loading. In Table 1 we list the regression coefficients for 3 different mid-latitude summer atmospheres where we only used path reflectance values when the total transmission of the atmosphere was above a certain threshold, e.g. 0.3. In Figure 8 we plot the path reflectance as a function of wavelength in a log-log plot, which shows that there seem to be two different slopes for visible channels versus SWIR channels.

We found that the method described works visually very well for a large number of AVIRIS derived scenes. True color composites using the red, green and blue atmospherically corrected reflectances were stretched equally over a pre-determined reflectance range. The resulting images show improved colors over vegetative and water surfaces. Further work is in progress to relate the fitting coefficients to atmospheric optical depth.

Aerosol Type	a_{vis}	b_{vis}	a_{swir}	b_{swir}
No Aerosol	-3.09	-4.15	-3.07	-4.05
23 km Rural	-1.99	-2.1	-1.96	-2.15
5 km Urban	-1.63	-1.22	-1.66	-1.74

Table 1. Fitting coefficients to the path reflectance in a mid-latitude summer atmosphere using MODTRAN 3.5 results for a DISORT calculation with 4 streams. The actual spectra are shown in Figure 8.

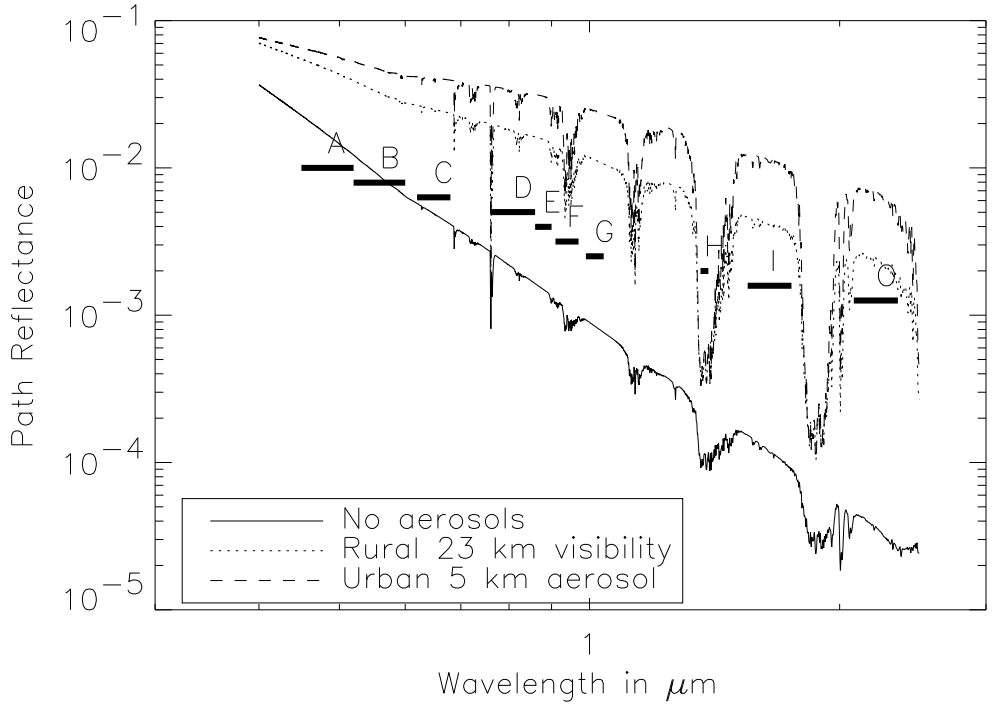

Figure 8. Top of atmosphere radiances for 10 MTI channels as a function of aerosol conditions.

4. Conclusions

We have described a few practical techniques to pre-process data for dark surfaces and screen clouds. Two methods were presented to atmospherically correct data using in-scene information over dark vegetation and water. We showed that atmospheric correction needs to be integrated with other retrievals and that it is a difficult area for multi-spectral sensors when there are no spectral channels dedicated to measure atmospheric parameters like the 0.94 μ water vapor band and the 1.38 μm cirrus band.

References

Borel, C.C., "Surface Emissivity and Temperature Retrieval for a Hyperspectral Sensor", IGARSS'98 conference in Seattle, WA, July 6-10, 1998.

Borel, C.C., W.B. Clodius, J.J. Szymanski and J. Theiler, "Comparing Robust and Physics-based Sea Surface Temperature Retrievals for high Resolution, multi-spectral Thermal Sensors using one or multiple Looks," SPIE'99 Aerosense conference, Orlando, 1999.

Chavez Jr., P.S., "An Improved Dark-Object Subtraction Technique for Atmospheric Scattering Correction of Multi-spectral Data," Remote Sensing of Environment, Vol. 24, pp. 459-479, 1988.

Chavez Jr., P.S., "Image-Based Atmospheric Corrections-Revisited and Improved," Photogrammetric Engineering & Remote Sensing, Vol. 62, 1996.

Diner, D.J., J.V. Martonchik, E.D. Danielson, and C.J. Bruegge, "Atmospheric Correction of High Resolution Land Surface Images," Proceedings, IGARSS '89 and the 12th Canadian Symposium on Remote Sensing, Canadian Remote Sensing Society, Vancouver, B.C., pp. 860-863, 1989.

Fraser, R.S. and Y.J. Kaufman, "The relative Importance of Aerosol Scattering and Absorption in Remote Sensing," IEEE TGARS, 23(5):625-633, 1985.

Gao, B.-C., and A.F.H. Goetz, "Cloud Area Determination from AVIRIS Data using Water Vapor Channels near 1 μm," JGR, 96(D2):2857-2864, 1991.

Gao B.-C., Heidebrecht K.B., and Goetz A.F.H., "Derivation of Scaled Surface Reflectance from AVIRIS Data," Remote Sens. Environ., 44:165-178, 1993a.

Gao, B.-C., Goetz, A.F.H., and Wiscombe, W.J., "Cirrus Cloud Detection from airborne Imaging Spectrometer Data using the 1.38 μm Water Vapor Band," Geophysical Research Letter, 20: 301-304, 1993b.

Gao, B.-C., Y.J. Kaufman, W. Han, and W.J. Wiscombe, "Correction of thin Cirrus Path Radiance in the 0.4-1 μm spectral Region using the i sensitive 1.375 μm Cirrus detecting Channel,", JGR-Atmospheres, 103(D24), pp. 32169-32176, 1998.

Gillespie, A.R., S. Rokugawa, S.J. Hook, T. Matsunaga, and A.B. Kahle, "Algorithm Theoretical Basis Document for Temperature/Emissivity Separation," Version 2.3, 16 August 1996.

Hook S.J., A.R. Gabell, A.A. Green and P.S. Kealy, "A Comparison of Techniques for Extracting Emissivity Information from thermal infrared Data for Geologic Studies," Remote Sens. Environ., 42, 123-135, 1992.

Kahle, A.B., D.P. Madura and J.M. Soha, "Middle infrared multispectral Aircraft Scanner Data: Analysis for geologic Applications," Applied Optics, 19(14):2279-2290, 1980.

Kaufman, Y.J., and Tanre, D., "Strategy for Direct and Indirect Methods for Correcting the Aerosol Effect on Remote Sensing: From AVHRR to EOS- MODIS," Remote Sens. Environ, 55:65-79, 1996.

Kneizys F.X., Abreu L.W., Anderson G.P., Chetwynd J.H, et al., "The MODTRAN 2/3 and LOWTRAN 7 Model," Philips Laboratory, prepared by Ontar Corporation, North Andover (MA), 267 pp, 1995.

Liang, S., H. Fallah-Adl, S. Kalluri, J. Jaja, Y. Kaufman, and J. Townshed, "An operational Atmospheric Correction Algorithm for Landsat Thematic Mapper Imagery over the Land," J. Geophys. Res., 102, 17173-17186, 1997.

O'Neill, N.T., J.R. Miller and J.R. Freemantle, "Atmospheric Correction of Airborne BRF to yield Surface BRF: Nomenclature, theory and methods," Can. J. Rem. Sens., 21(3):309-327.

Pinty, B. and M.M Verstraete, "GEMI: an non-linear Index to Monitor global Vegetation from Satellites," Vegetatio, 101:15-20, 1992.

Richter R., "A Spatially Adaptive Fast Atmospheric Correction Algorithm," Int. J. of Remote Sensing, 17(6): 1201-1214, 1996.

Richter, R., "Correction of Satellite Imagery over mountainous Terrain," Applied Optics, 37, 1998.

D. Schlaepfer, C.C. Borel, J. Keller and K.I Itten, "Atmospheric Pre-corrected Differential Absorption Technique to retrieve columnar Water Vapor", RSE Vol. 65, no. 3, pp353-366, 1998.

Teillet, P.M., and Fedosejevs, G., "On the Dark Target Approach to Atmospheric Correction of Remotely Sensed Data," Canadian J. of Remote Sensing, 21, 1995.

Tornow, C, "Anwendung fractaler Methoden zur Abschätzung der aerosol-optischen Tiefe für die Atmosphärenkorrectur räumlich hochaufgelöster Satellitendaten," Dissertation, Freie Universität Berlin, 1992.

Tornow, C., C.C. Borel and B.J. Powers, "Robust Water Temperature Retrieval using multi-spectral and multi-angular IR Measurements," IGARSS'94, Pasadena, pp.441-443.

Vermote E., Tanré D., Deuzé J.L., Herman M., and Morcette J.J., "Second Simulation of the Satellite Signal in the Solar Spectrum," 6S User Guide, NASA-Goddard Space Flight Center, Greenbelt (MD), 182 pp., 1994.